RESEARCH ARTICLE | JANUARY 03 2023

High-resolution micro-cavity filling sensing by fiber optic interferometry

Majid Fazeli Jadidi ; Zahra Gholamvand ; Graham L. W. Cross

Rev. Sci. Instrum. 94, 015001 (2023)
https://doi.org/10.1063/5.0109751

Review of Scientific Instruments ARTICLE scitation.org/journal/rsi

High-resolution micro-cavity filling sensing by fiber optic interferometry

Cite as: Rev. Sci. Instrum. 94, 015001 (2023); doi: 10.1063/5.0109751
Submitted: 14 July 2022 • Accepted: 8 December 2022 •
Published Online: 3 January 2023

Majid Fazeli Jadidi,[1,2,3] Zahra Gholamvand,[1,2,3] and Graham L. W. Cross[1,2,3,a)]

AFFILIATIONS

[1] Adama Innovations, CRANN, Trinity College Dublin, Dublin 2 D02W085, Ireland
[2] Advanced Materials and Bioengineering Research (AMBER) Centre, CRANN, Trinity College Dublin, Dublin 2 D02W085, Ireland
[3] School of Physics, Trinity College Dublin, Dublin 2 D02PN40, Ireland

[a)] **Author to whom correspondence should be addressed:** graham.cross@tcd.ie. **Tel.:** +353 (0)1 896 3024

ABSTRACT

In the last decade, new potential applications of micro- and nano-products in telecommunication, medical diagnostics, photovoltaic, and optoelectronic systems have increased the interest to develop micro-engineering technologies. Injection molding of polymeric materials is a recent method being adapted for serial manufacturing of optic components and packaging at the micro- and nano-scale. Quality assurance of replication into small cavities is an important but underdeveloped factor that is needed to ensure high production efficiency in any micro-fabrication industry. In this work, we introduce a fiber-based interferometric measurement sensor to monitor the cavity filling of optical microstructures fabricated into a macroscopic molding die. The interferometer was capable of resolving melt front motion into the microcavity to the point of complete filling as verified by atomic force microscopy. Despite the low reflectivity of the transparent polymer and unoptimized reflected light collection optics, this system is capable of monitoring polymer movement during the course of filling and detecting the completion of the process. The simplicity and flexibility of the technology could allow eventual instrumentation of injection molds, embossing, and nanoimprint tooling suitably modified with a small optical window to accommodate light from an optical fiber. This would provide a solution to the challenging problem of monitoring local, nanometer scale filling processes.

I. INTRODUCTION

The feasibility of products manufactured with low cost, high functionality, and the decreased feature size is a demanding industrial trend. Recent breakthroughs in manufacturing technology for micro-devices demand materials to be compatible, economically affordable, and allow high throughput for mass production. Injection over-molding of polymeric material is a recent method in the serial manufacturing of optoelectronic components and medical devices at the micro and nanoscale.[1,2] Advantages of injection mold processing include high throughput, ease of control of process parameters, low fabrication cost, and the wide flexibility of shapes that can be formed.[3–5] Quality control during the replication process plays a key role in any micro-fabrication technology and is the focus of this research: The effectiveness of replicated micro-features in a combined micro-device is significantly determined by the quality of fabrication. In replicated micro-products, this is strongly reliant on the fidelity of its dimension with the desired shape and size of the micro-feature. Process monitoring using a fully transparent or specially window-modified mold in a pre-production test to monitor mold microcavity filling by the melt flow during the replication process may be of great value. Factors affecting macroscopic melt flow in conventional injection molding include injection speed, pressure, melt, and mold temperature.[6–11] At small scales, new factors like surface tension can also play a role.[12] The use of this monitoring technique in a pre-production test will provide a clear understanding of the effect of set parameters to increase the efficiency of filling of micro and nanoscale features in the injection molding and hot embossing processes. Eventually, our sensing method may be used as an in-line mold filling sensor if the main mold in the injection molding process is made from a transparent material such as sapphire or fused quartz or if the metallic mold is made with a transparent window to be monitored by an optical beam. The quality control during pre-process micro-injection molding will enable the operator

to monitor the flow of the polymer melt into micro-cavities, stop the uncompleted replication at any stage, and change the set parameters of the process to reach the best state.

Time Resolved Diffraction Scatterometry (TRDS) is an example of optical metrology for measuring the filling of large, regular arrays of nano-patterns for nanoimprint lithography.[13] Here, we propose fiber-based interferometry as a nanoscopic mold-filling sensor for compatibility with injection molding machinery and the ability to address a single microcavity. Fiber-optic interferometry (FOI) was developed for use in atomic resolution Atomic Force Microscopy (AFM) to measure the deflection of micro-cantilevers.[14,15] The FOI system has outstanding sensitivity and allows measurement of displacements to sub-Angstrom displacement levels.[16,17] We show that the FOI technique can monitor the movement of a polymeric melt surface by detecting the start and completion stage of the filling process, demonstrating the capability of this system to be used as a mold filling sensor for injection over-molding of microscopic cavities. FOI detection system will enable the operator to simply point out the completed and uncompleted replications during injection molding if the mold is either fully transparent or possess a window suitably transparent to the optical beam with a kind of simple "thumbs up, thumbs down" indicators.

II. MATERIALS AND METHODS

Materials with transparency in Near Infrared (NIR) regime were evaluated in terms of suitability for FOI sensing and injection molding process. Properties, such as hardness, surface smoothness, durability, and integrity at high temperatures, low surface adhesion, high thermal conductivity, and a long lifetime must be considered to select the most suitable materials for manufacturing the molds in the injection molding industry. For this work, glass, sapphire, and fused quartz were considered suitable materials.

We used a three-step patterning technology combining optical lithography, dry plasma etching, and electron beam evaporation coating to create micro scale features on transparent substrates as test molds. The fabrication process is schematically illustrated in Fig. 1. The sample was coated with an S1813 G2 positive photoresist layer via spin coating to form a mask for plasma etching. Exposure of the photoresist was made by UV light irradiation through a structured optical photomask contacted to the photoresist by a mask

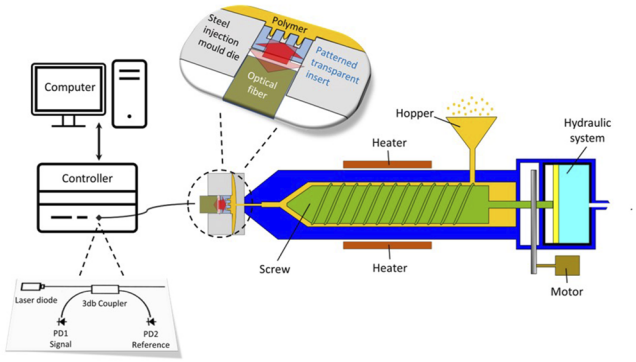

FIG. 2. Schematic of the integrated in-line quality control system for the injection molding based on a fiber-delivered optical reflectance measurement.

aligner and then immerse into the chemical developer (MF319), agitate gently for about 45 s to remove the photoresist exposed to UV light, and provide a patterned resist layer on the sample. The patterned surface is then subject to plasma etching (Ar-CHF3) such that the sample materials below the structured resist-free regions can be removed to a specific depth. Then, the entire patterned and etched surface was coated first with a 2 nm titanium adhesion layer followed by 20 nm gold to introduce a semi-reflecting layer within the cavities. The last step is to remove the residual photoresist layer by washing it with acetone, leaving a pattern transfer of metalized cavities behind. Optical images of microfeatures on a glass slide with relief of ~1.4 μm and in plane width ranging from 5 μm to 1 mm are shown in Figs. 1(e) and 1(f).

Our detection system consisted of a Fabry–Pérot interferometer[14] coupled to an optical fiber with an end positioned above the back side of the transparent mold. This specially designed sensing unit consists of a laser diode operating at a constant power at the wavelength of 1310 nm that is coupled into a 50% single-mode fiber splitter. A single-mode fiber positioned very close to the moving target is connected to one of the fiber splitters outputs. The other output and the input of the splitter are connected to the reference and signal photodiodes, respectively (see Fig. 2). The laser power is

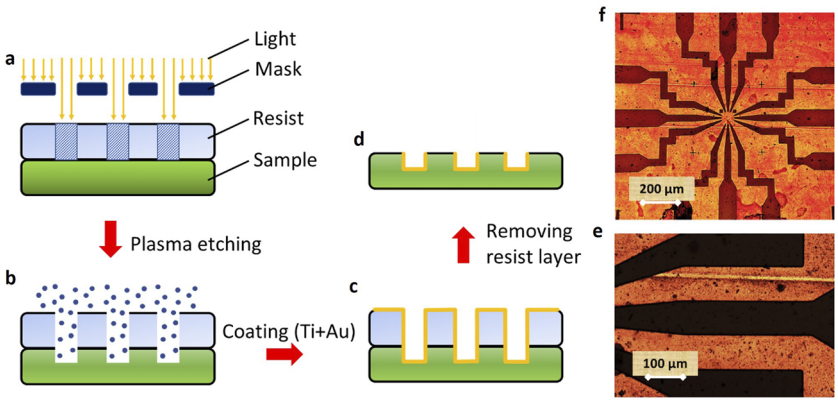

FIG. 1. (a)–(d) Schematics show the steps of the masked plasma patterning process on glass and quartz samples. (f) Example of multiscale features formed into the glass for this study with zoom-in is shown in (e).

measured with the output of the reference photodiode, and consequently, the laser power fluctuations and laser intensity noise are subtracted from the output of the signal photodiode. Beams reflected from the interfaces at constant positions including the fiber end-face and surface of a moving target form an interference signal that is monitored using the signal photodiode. The distance between two peaks in the interference pattern is the half-wavelength of the laser when the gap is air. The change in power of the interference signal can be accurately converted to the displacement of the target in a calibrated system.

III. THEORY

Reflectance and interference of reflected optical beams in a multilayer system depend on the optical characteristics of layered materials. The signal intensity of interfering beams in the cavity of the Fabry–Pérot interferometer with multiple beam reflections and with nominal intensity I_0 is[15]

$$I = I_{noise} + I_0 \frac{Fsin^2(\varphi)}{1 + Fsin^2(\varphi)}, \quad (1)$$

where I_{noise} is the offset noise of the signal, the finesse F, and φ is the phase difference that can be calculated from the thickness of Fabry–Pérot cavity t, optical constant n of the medium in the cavity, and the wavelength of light λ by $\varphi = (2\pi/\lambda)nt$. However, the interference signal in a multilayer system including a metallic layer cannot be calculated effectively by formula (1) due to the increased complexity of the behavior of metallic layers with electronic absorption. Ruf *et al.*[15] considered the multilayer system with metallic layers and introduced a formula that can be used to simulate the interference signal with better approximation. Recently, Byrnes[18] derived a formula from the Fresnel equations that calculates the optical properties of light interaction with a multilayer planar stack. He used the transfer-matrix method that is based on the product of characteristic matrices M_i of every single layer of the multilayer system. This calculation is provided with the "tmm" Python software package (tmm 0.1.8), which is used in this work to simulate the interference signal to be monitored with the fiber optic interferometry technique in the injection molding process.

IV. RESULTS AND DISCUSSION

A. Theoretical simulations

We simulated a one-dimensional (1D) model of the optical reflection of moving target material in a multilayer planar stack system similar to our melt front mold setup. Figure 3 shows the calculated interference signals between beams reflected from a downward moving target [a fully reflecting gold mirror in Figs. 3(a) and a semi-transparent polycarbonate sheet in Fig. 3(b)] and a fixed position interface below it. The optical constants of layered materials were taken from bulk materials for the calculation of the interfer-

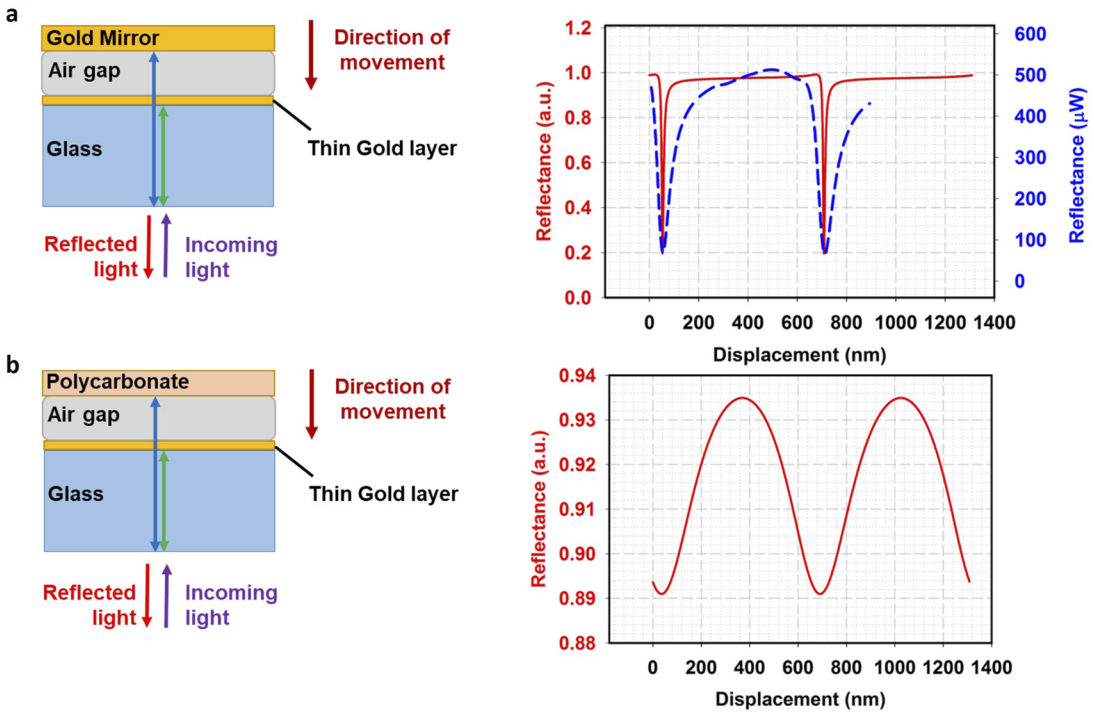

FIG. 3. (a) The calculated reflectance signal when a gold mirror approaches the surface of a glass coated with a thin layer of gold is shown as a solid red line, while a blue dashed line graph corresponds to the reflectance signal measured in the experiment. (b) The calculated reflectance signal when a polycarbonate sheet approaches the gold coated glass surface.

ence signal.[19–21] Deviation of the shape of the interference signal from a simple sinusoid is due to the multiple reflections in the Fabry–Pérot cavity and complex optical constants of metallic films.[15] The optical characteristics of layered materials play the main role in the symmetry of the interference signal. While materials, such as polymers, have a refractive index that is almost real (with a very low extinction coefficient), metals have a complex refractive index component with a considerably greater absorption (i.e., extinction) coefficient.[15,19–21] The absorption coefficient in the complex optical constants of metallic materials is the main reason for the asymmetric shape of the interference signal.[15] The wavelength of fringes in the periodic pattern of monitored interference signal depends on the refractive index of the material in the gap between the moving target and the surface at the constant position at the bottom of the cavity. Normally, this gap will be air with a refractive index of ~1, resulting in half the wavelength of the incident laser beam as a distance between each periodic pattern. This provides a possibility to monitor and measure the relative movements of target material via fiber optic interferometry. The FOI technique has been used in high resolution AFM instruments where the short-distance travel (up to ~10 nm) of a bending cantilever can be measured by locking at the proper quadrature point of the interference pattern and keeping it at the highest slope position. This can provide measurements with sub-Angstrom spatial resolution.[14,16,17] The wavelength of the interference pattern is independent of its shape, meaning that it can be used to measure long-distance movements by counting the number of interference oscillations. While estimating sub-wavelength displacements for metallic interference patterns like Fig. 3(a) can be challenging for FOI, for non-metallic materials without an absorption coefficient in its optical constants, the symmetric shape in the interference signal can enable tracking movements to nanometer accuracy.

The lateral spatial resolution of the filling front monitored by the FOI technique will vary with the thickness of the transparent mold due to beam divergence. This is because the core diameter of the single mode fiber in our sensing system is only ~9 μm, thus only a fraction of back-reflected light will be collected by the fiber to be fed back into the interferometer. This can be seen in Fig. 4 where the incident fiber light spreads out as the upward beam in brown, while only the dark green part of the full reflected light shown in light green is captured. The beam divergence in a specific medium with optical constant n_m and thickness z can be calculated by[22]

$$R^2(z) = R_0{}^2\left[1 + \left(\lambda z/\pi n_m R_0{}^2\right)^2\right], \quad (2)$$

where the R_z, R_0, and λ are the radius of the diverged beam, the mode field radius of the fiber, and the wavelength of the beam, respectively. The divergence of our beam at the surface of a glass mold with 1 mm thickness is ~120 μm, and the reflected beam divergence at the bottom surface of the glass where it could be received by fiber is ~240 μm. Considering that the fiber core is 9 μm in diameter, the proportional area on the upper surface of the glass where the entire reflected beam from it can be received by the fiber is around 4.5 μm. To improve the spatial coverage at the mold surface, optical collimators or focusing components compatible could be used to collect more light and increase the signal-to-noise ratio. However, the high temperature nature of injection molding processes makes it challenging to provide collimators with the objectives operating at temperatures as high as 200 °C.

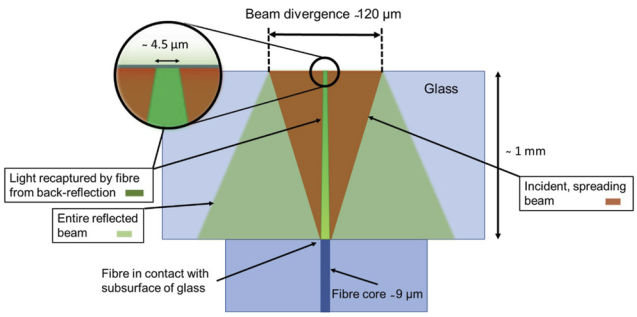

FIG. 4. Schematic showing calculated beam divergence of 120 μm (brown) at the top surface of the glass mold window of 1 mm thickness. Only a limited region of 4.5 μm wide of the back-reflected beam light (shown in light green) is actually received by the fiber, as shown in dark green.

B. Experimental results

The laboratory functionality test of this system, which simulates the actual injection molding process, was performed by measuring the polymer's melt front displacement (filling) using non-contact thermal heating of a polymer (Polyvinyl acetate) with the monitored interference of reflected signals. A schematic of our fiber optical interferometric measurement of polymer melt filling of a glass mold is shown in Fig. 5(a). To simulate mold cavity filling, we used a patterned glass slide with microstructures of various lateral dimensions ranging from 5 μm to 1 mm with relief of 1.4 μm shown in Figs. 1(e) and 1(f). The polymer pellet was melted using a non-contact heating method. Polyvinyl acetate (M_w:83 000, Sigma-Aldrich) was chosen as a convenient material due to its low melting temperature (Tg ~35 °C). This also minimized the effects of differential thermal expansion of the mold in the monitored interference signal. The polymer pellet was placed and heated on the microstructure to get melted and fill the cavity by merely the gravity force and capillary forces. The gold coated structured glass mold and melted polymer on the mold are shown in Figs. 5(b) and 5(c). Figure 5(d) shows the optical reflection measurement result of polymer melt filling into a glass mold cavity with a width of 1 mm and a depth of 1.4 μm at a point, which is indicated by a red dot in Fig. 5(b). This is compared to a control signal that is shown in Fig. 5(e), measuring only the effect of thermal expansion on the mold when the experiment is repeated with the polymer-free heating process. By analyzing the polymer's filling signal vs the control, we can identify the movement of the polymer into the cavity and completion of the filling process as a leveling off the signal oscillations with time [as indicated by the red arrows in Fig. 5(d)] while the long-range change in the monitored reflection signal (background effect) is due to thermal expansion of glass mold. The background effect is subtracted from the measured interference signal, which is shown in Fig. 5(f). A periodic pattern in the interference signal followed by the constant level, respectively, indicates the progress and completion of the filling process. The displacement of the polymer into the cavity is extracted from the pattern in the measured interference signal. One period of the fringes in

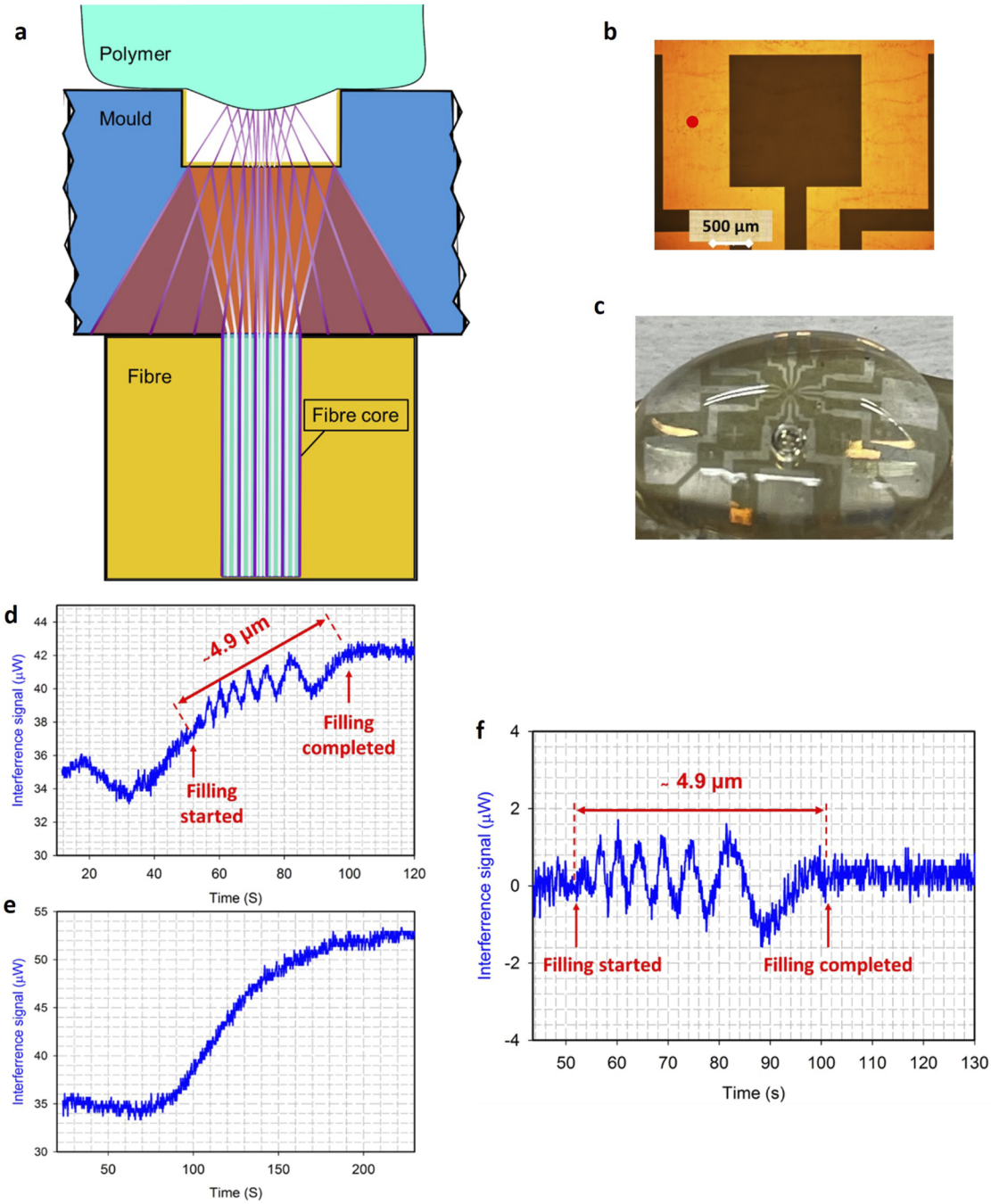

FIG. 5. (a) The illustrating schematic of polymer melt front test (not to scale). (b) The gold coated and structured glass mold where the fiber delivered filling measurement was carried out. (c) Molten polymer on the glass mold. (d) Measured interference signal during the polymer melt filling process at a point, which is indicated by a red dot in (b). The filling start and completion points are indicated with red arrows on the graph. (e) Background effect on the monitored signal due to thermal expansion of glass. (f) Background subtracted reflection signal with fringes corresponding to the movement of polymer into the mold.

the interference signal corresponds to a distance of 655 nm (half the wavelength of the incoming infrared laser beam), which enables us to measure the movement of the polymer into the cavity. Seven full and one-half fringes with very slightly growing amplitudes can be observed in the measured reflection signal. The relative movement of polymeric melt corresponding to the seven and a half observed fringes is about 4.9 μm. The difference in the measured displacement of molten polymer and mold depth is due to the surface roughness of

the polymer pellet where the monitored point at the polymer front surface was placed at a level of height on top of the glass mold before getting heated.

To attempt to remove the background effect from the monitored signal, the test was repeated with more rapid heating of the polymer. This allowed the filling process to complete while transferring significantly less heat to the entire glass mold and reducing overall thermal expansion effects. A microcavity of width 100 μm and depth 1.4 μm was used. In Fig. 6(a), we plot the interferometer signal from the first observation of a signal above the noise level to the cessation of changing vs time as the cavity was filling with molten polymer (indicated by red arrows). We observe almost five complete fringes of growing amplitude in the interference signal without the background effect transitioning to a constant level with time, which we interpret as the progress and completion of the filling process.

As the melt front approaches the cavity floor, the visibility of the interference fringes rises above the noise floor 0.9 μW to reveal five fringes in total. The relative movement of polymeric melt corresponding to the five observed fringes is about 3.3 μm. An analysis via monitored interference signal [shown in Fig. 6(a)] of the last fringe before contact gives a displacement resolution of ~60 nm. In principle, by fitting the flatline and fringe sections of the data, the resolution could be improved to the nanometer level (estimated). The measured relief in the structured glass mold of 1.4 μm implies that we measured the polymer front well before the point that it entered the cavity. This is thought to be due to the intrinsic roughness of the polymer pellet that was placed on top of the mold before melting. The replicated polymer from an instrumented molding experiment is shown in Fig. 6(b). In Fig. 6(c), the displacement of the polymer filling front vs time is extracted from the interference signal of Fig. 6(a). The schematics in this figure indicate the estimated progression of filling. As explained above, the melt front monitoring at the surface of the mold cavity is estimated to be for a region less than 5 μm in size in the central region. Detection of filling completion, particularly at the corners of such a large structure as 100 μm, will need further improvements with modified optics. Thus, the last schematic showing the completion of the filling process at the corners of the cavity is an estimation only. However, complete filling in this test was confirmed by atomic force microscope (AFM) imaging of the replicated structure as shown in Figs. 6(d) and 6(e). The AFM image and line profile indicate that although the detection signal is collected only from a small, central area, an accurate estimation of filling completion can be made.

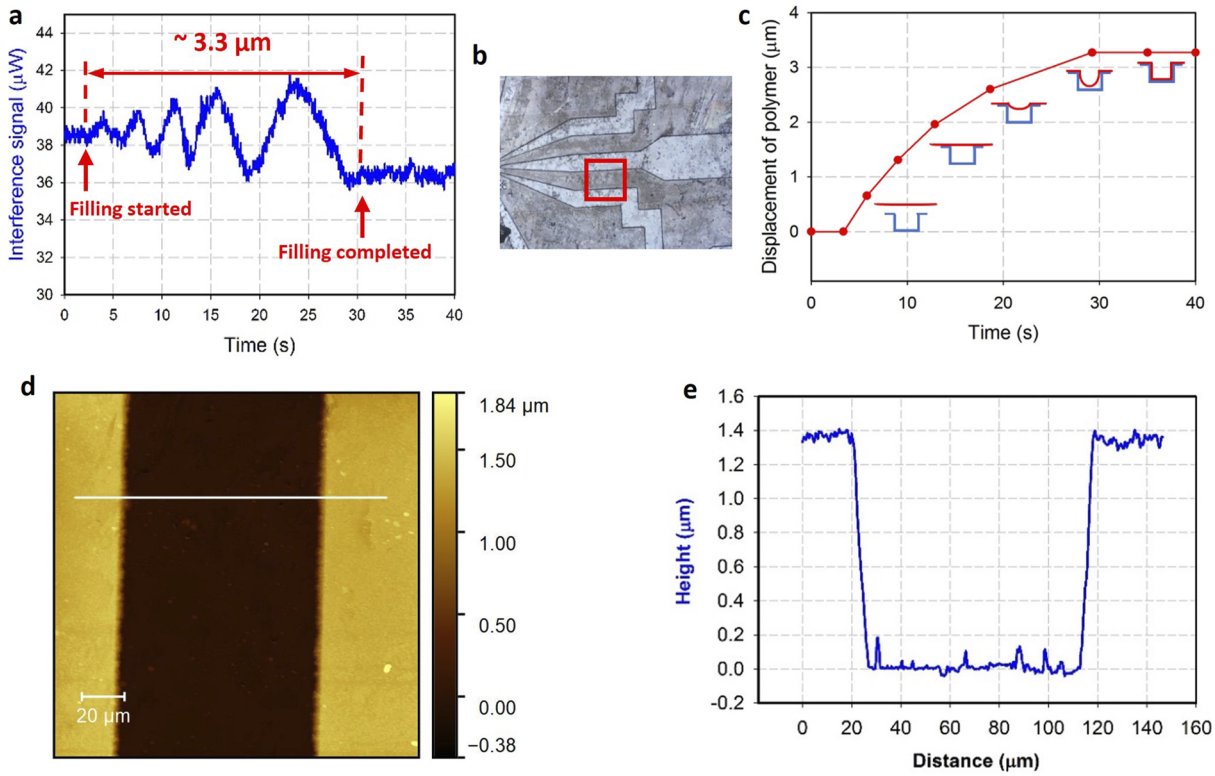

FIG. 6. (a) Measured interference signal during the polymer melt filling process. The filling start and completion points are indicated with red arrows on the graph. (b) Optical microscope image of the replicated polymer where the red square indicates the scanned region with AFM. (c) The displacement of the polymer filling front with time extracted from the measured interference signal is shown in (a) where the schematics show the estimated progression of the filling process. (d) AFM image obtained from the shaped structure on the replicated polymer. The scanned area is indicated by a red square in (b). (e) Line profile over the indicated region with the white line on the AFM image.

Our 1D model of the optical Fabry–Pérot (FP) cavity is an idealization that will, in reality, be influenced by the evolving three-dimensional shape of the filling mold cavity. This will affect both the intensity of the FP signal and its lateral resolution. The interference fringes in the FP signal are a result of the superposition of a complex set of reflections from surfaces of the filling cavity ultimately related to the movement of the polymer filling front and static cavity walls. However, for materials, such as polymers with small reflection coefficients, the effect of multiple reflections in a cavity of the FP system can be neglected.[23] Wilkinson and Pratt[23] studied fiber Fabry–Pérot interferometers for various materials with different reflection coefficients. For materials with a small reflection coefficient, they showed an amplitude of interference fringes that slightly increased as the distance between the material and the fiber approached zero. In the 1D computation shown in Fig. 3, the absence of any lateral dimension of fiber and layers or reflection results in the amplitude of the simulated fringes being constant with filling. However, in reality, a gradual increase in the amplitude of the fringes is expected to be seen as the partially filled mold cavity changes shape: The greater fraction of reflected beams from the polymer will be received by fiber as the polymer approaches the bottom of the mold, as shown by the schematic diagrams in Figs. 7(a)–7(c), respectively.

Two different trends were observed in the results of two different experiments shown in Figs. 5(f) and 6(a). While a slight growth of interference fringes can be seen for the reflection measurement of polymer melt front test on a cavity with 1 mm width [Fig. 5(f)], a relatively sharper increase in the amplitudes of the fringes can be

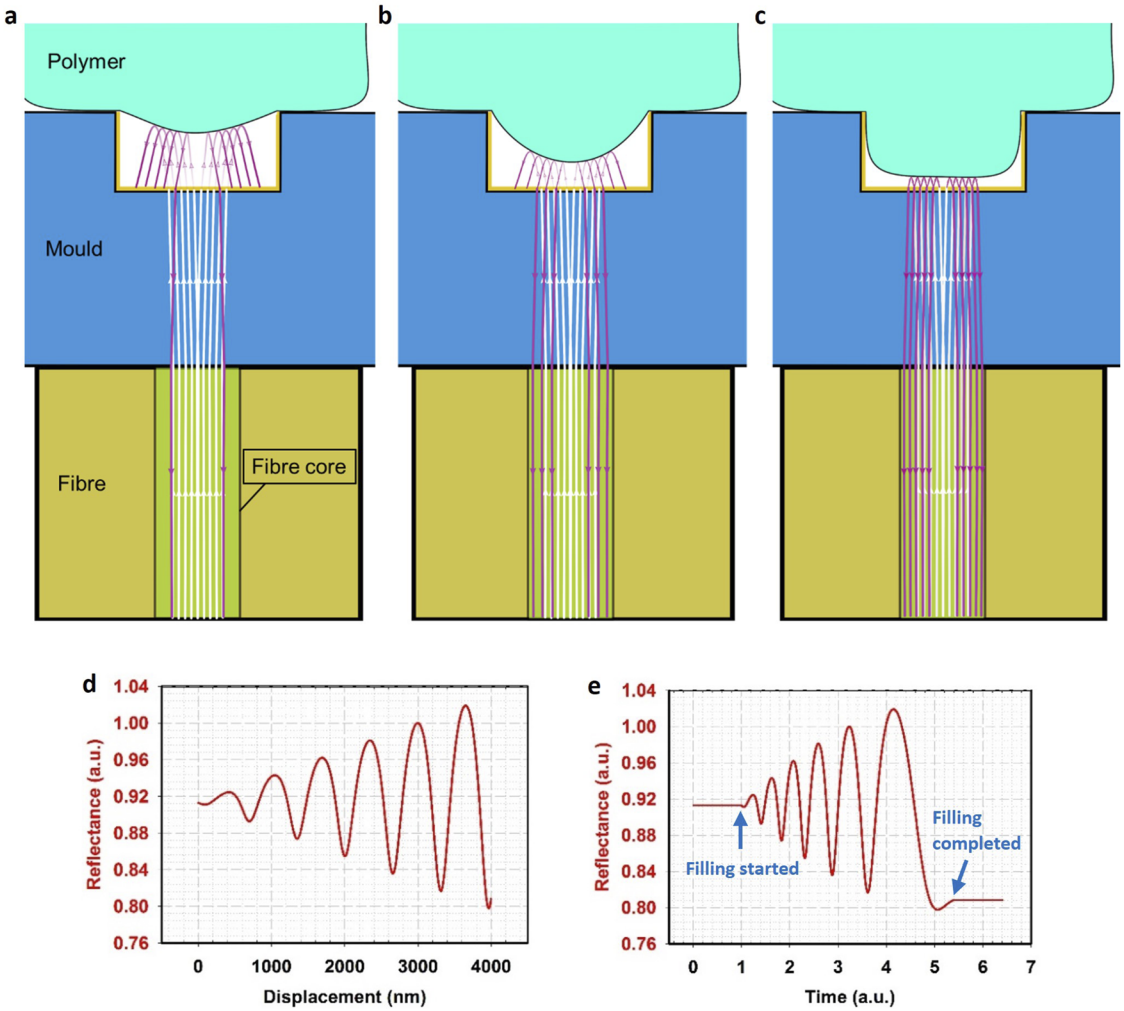

FIG. 7. (a)–(c) Illustrating schematics showing how the larger portion of the reflected beams from moving polymer can be received by fiber as polymer filling into the mold. The incoming beams and reflected beams are indicated with white and purple colors, respectively. (d) A simulated reflection signal from a polymer material with a growing amplitude of the fringes indicates the progress of the filling process. (e) A simulated reflection signal vs time that can be monitored by the fiber interferometry detection setup showing the start point, course of progress with growing fringes, and completion points of polymer filling in an injection molding process.

observed for a test on a cavity with 100 μm width [Fig. 6(a)]. We think that the shape of the polymer front surface plays a considerable role in this effect. The curvature of the polymer front surface can depend on the width-to-depth ratio of the local mold cavity, the size of the main mold behind the micro-cavity, and mold-polymer interfacial energy.[24] As the width-to-depth ratio of a cavity is increased, the path of the polymer into the cavity can even be changed from center-first to the sidewalls, especially in narrow nanoimprint type geometries. For our wide-open injection mold type geometry, at the initial stage of filling, we expect that the polymer front at the center is close to a flat surface. However, the curvature will increase as the polymer fills as shown in Figs. 7(a) and 7(b). Then, at the final stages of filling, the curvature of the polymer front at the center may flatten again as shown in Fig. 7(c). These effects can explain the modulation of the interference amplitude we observe in our data: We expect the effects of an increase in curvature to be most pronounced in the narrower cavities, which are shown in Fig. 6(a), while the second reversal of curvature may appear is less effective for wider cavities like we see in Fig. 5(f) where the growth in amplitude is insignificant.

In general, a greater portion of the rays reflected from the polymer will be received by the fiber as the polymer approaches the bottom of the cavity. This will result in an overall increase in the amplitude of the fringes in the reflection signal followed as the polymer fills the mold. Figure 7(d) shows an estimate of the reflection signal when a polymer is filled into the mold in the injection molding process. A gradual increase in the amplitude of the oscillations in the traced reflection signal is a reliable indicator of the direction of movement of the polymer to fill the mold at any given step of the filling process.

The completion of the filling process can be identified by an abrupt cessation in any variation of the interference signal vs time in the traced reflection signal, as seen in our data [Figs. 6(a) and 5(f)] and illustrated by the simulation [Fig. 7(e)]. Gradual changes during injection near the completion of filling can be considered as a signal that the cavity is not filled, even though the exact interpretation of the signal does not fit with a simple 1D model of a moving filling front. In Fig. 7(e), we assume a linear slow-down in filling rate in representative fringe-amplitude vs time signal. This means that the fringe period on the time scale can be increased, but each fringe corresponds to a constant displacement of 655 nm, which is half the wavelength of the light used. Finally, we note that the fluctuations in the filling signal may continue even when the central part of the filling front is arrested by contact with the cavity while the corner regions continue to fill. The highly transparent polymer may allow some reflections from moving surfaces at the corners to re-enter the fiber until all cavity walls come into contact. We will investigate this further in future work.

V. CONCLUSION

We have successfully introduced fiber optic interferometry as an in-mold monitoring system of the filling process during the injection molding of polymeric materials. This sensing technique can be used as a pre-production filling test unit or as an in-line filling sensor if the mold is modified to be either fully transparent or possess a window suitably transparent to the optical beam. This optical system shows sufficient sensitivity even with the very low reflectance of the moving polymer melt front. The system provides sufficient detectability to trace the course of the filling process and to allow "fill/no-fill" type decisions to be made by observing when the signal ceases changing. The sensitive region for melt front monitoring at the surface of a 1 mm thick mold with a 100 μm wide, 1.4 μm deep cavity was estimated to be <5 μm. Our melt front monitoring system may eventually be useful to measure filling for a range of surface structures with nanometric relief and micrometer lateral dimension. The signal to noise ratio and corresponding vertical spatial resolution, as well as lateral spatial sensitivity, could be improved by incorporating lenses to focus and increase the collection of reflected light.

ACKNOWLEDGMENTS

This work was supported by the European Commission (Grant No. 820661—FLOIM—H2020-NMBP-TR-IND-2018-2020/H2020-NMBP-FOF-2018).

AUTHOR DECLARATIONS

Conflict of Interest

All authors contributed equally to this work.

Author Contributions

Majid Fazeli Jadidi: Investigation (equal); Methodology (equal); Writing – original draft (equal); Writing – review & editing (equal). **Zahra Gholamvand**: Investigation (equal); Writing – original draft (equal); Writing – review & editing (equal). **Graham Lawrence William Cross**: Conceptualization (lead); Resources (lead); Supervision (lead); Writing – original draft (equal); Writing – review & editing (equal).

DATA AVAILABILITY

The data that support the findings of this study are available from the corresponding author upon reasonable request.

REFERENCES

[1] U. M. Attia, S. Marson, and J. R. Alcock, "Micro-injection moulding of polymer microfluidic devices," Microfluid. Nanofluid. **7**, 1–28 (2009).

[2] H. Zhang, N. Zhang, W. Han, M. D. Gilchrist, and F. Fang, "Precision replication of microlens arrays using variotherm-assisted microinjection moulding," Precis. Eng. **67**, 248–261 (2021).

[3] B. Sha, S. Dimov, C. Griffiths, and M. S. Packianather, "Investigation of micro-injection moulding: Factors affecting the replication quality," J. Mater. Process. Technol. **183**, 284–296 (2007).

[4] C. Yang, X.-H. Yin, and G.-M. Cheng, "Microinjection molding of microsystem components: New aspects in improving performance," J. Micromech. Microeng. **23**(9), 093001 (2013).

[5] H. Zhang, F. Fang, M. D. Gilchrist, and N. Zhang, "Filling of high aspect ratio micro features of a microfluidic flow cytometer chip using micro injection moulding," J. Micromech. Microeng. **28**(7), 075005 (2018).

[6] D. Yao and B. Kim, "Increasing flow length in thin wall injection molding using a rapidly heated mold," Polym.-Plast. Technol. **41**(5), 819–832 (2002).

[7]B. R. Whiteside, M. T. Martyn, and P. D. Coates, "In-process monitoring of micromoulding – Assessment of process variation," Int. Polym. Process. **20**(2), 162–169 (2005).
[8]J. Zhao, R. H. Mayes, G. Chen, H. Xie, and P. S. Chan, "Effects of process parameters on the micro molding process," Polym. Eng. **43**(9), 1542–1554 (2003).
[9]A.-C. Liou and R.-H. Chen, "Injection molding of polymer micro- and sub-micron structures with high-aspect ratios," Int. J. Adv. Manuf. Technol. **28**(11), 1097–1103 (2006).
[10]F. Baruffi, M. Gülçür, M. Calaon, J.-M. Romano, P. Penchev, S. Dimov, B. Whiteside, and G. Tosello, "Correlating nano-scale surface replication accuracy and cavity temperature in micro-injection moulding using in-line process control and high-speed thermal imaging," J. Manuf. Process. **47**, 367–381 (2019).
[11]C. A. Griffiths, S. S. Dimov, S. G. Scholz, G. Tosello, and A. Rees, "Influence of injection and cavity pressure on the demoulding force in micro-injection moulding," J. Manuf. Sci. **136**(3), 031014 (2014).
[12]G. L. W. Cross, "The production of nanostructures by mechanical forming," J. Phys. D: Appl. Phys. **39**, R363 (2006).
[13]Z. Yu, H. Gao, and S. Y. Chou, "*In situ* real time process characterization in nanoimprint lithography using time-resolved diffractive scatterometry," Appl. Phys. Lett. **85**, 4166–4168 (2004).
[14]A. Oral, R. A. Grimble, H. Ö. Özer, and J. B. Pethica, "High-sensitivity non-contact atomic force microscope/scanning tunneling microscope (nc AFM/STM) operating at subangstrom oscillation amplitudes for atomic resolution imaging and force spectroscopy," Rev. Sci. Instrum. **74**(8), 3656–3663 (2003).
[15]A. Ruf, M. Abraham, J. Diebel, W. Ehrfeld, P. Güthner, M. Lacher, K. Mayr, and J. Reinhardt, "Integrated Fabry–Perot distance control for atomic force microscopy," J. Vac. Sci. Technol., B **15**(3), 579–585 (1997).
[16]M. F. Jadidi, U. Kamber, O. Gürlü, and H. Ö. Özer, "Investigation of CVD graphene as-grown on Cu foil using simultaneous scanning tunneling/atomic force microscopy," Beilstein J. Nanotechnol. **9**, 2953–2959 (2018).
[17]H. Ö. Özer, S. J. O'Brien, A. Norris, J. E. Sader, and J. B. Pethica, "Dissipation imaging with low amplitude off-resonance atomic force microscopy," Jpn. J. Appl. Phys. **44**(7S), 5325 (2005).
[18]S. J. Byrnes, "Multilayer optical calculations," arXiv:16030.02720 (2016).
[19]E. D. Palik, *Handbook of Optical Constants of Solids* (Academic Press, 1998).
[20]R. L. Olmon, B. Slovick, T. W. Johnson, D. Shelton, S.-H. Oh, G. D. Boreman, and M. B. Raschke, "Optical dielectric function of gold," J. Phys. Rev. B **86**(23), 235147 (2012).
[21]X. Zhang, J. Qiu, X. Li, J. Zhao, and L. Liu, "Complex refractive indices measurements of polymers in visible and near-infrared bands," Appl. Opt. **59**(8), 2337–2344 (2020).
[22]O. Svelto, "Properties of laser beams," *Principles of Lasers* (Springer, 2010), pp. 475–504.
[23]P. R. Wilkinson and J. R. Pratt, "Analytical model for low finesse, external cavity, fiber Fabry–Perot interferometers including multiple reflections and angular misalignment," Appl. Opt. **50**(23), 4671–4680 (2011).
[24]H. D. Rowland and W. P. King, "Polymer deformation and filling modes during microembossing," J. Micromech. Microeng. **14**(12), 1625 (2004).